Sex and regional differences in microglia morphology and complement receptor 3 are independent of constitutive neuroinflammatory protein concentrations in healthy mice.

Authors: Kimberly Young[1], Janet Rothers[1], Sergio Castañeda[2], Jenna Ritchie[2], Ayumi E. Pottenger[3], Helena W. Morrison[1 *]

Kimberly Young, youngk1@email.arizona.edu
Janet Rothers, rothers@email.arizona.edu
Sergio Castañeda, sergiosalguero@email.arizona.edu
Jenna Ritchie, jennaritchie@email.arizona.edu
Ayumi E. Pottenger, apottenger@email.arizona.edu
Helena W. Morrison, hmorriso@email.arizona.edu

[1] University of Arizona, College of Nursing, 1305 N. Martin Ave, P.O. Box 210203 Tucson, AZ 85721

[2] University of Arizona, College of Science, Department of Neuroscience, 1040 E 4th Street PO Box 210077, Tucson, AZ 85721

[3] University of Arizona, College of Science, Department of Molecular and Cellular Biology, 1007 E. Lowell Street, PO BOX 210106, Tucson, AZ 85721

* Correspondence
Dr. Helena Morrison
hmorriso@email.arizona.edu

Running Title: Sex and brain region microglia

Keywords: Microglia, complement receptor 3, accelerated ovarian failure, neuroinflammation

Abstract

Microglia are highly ramified brain phagocytes that are finely tuned to surrounding neuronal and glial activity. Combined, microglia morphology, dynamic process movement, phagocytic, and neuroinflammatory responses aid in the detection of changed neuronal function, maintenance, and restoration of neural networks during physiology and pathophysiologic conditions. An awareness of how microglia diversity in the healthy brain relates to brain region and sex differences would inform brain physiology, further delineate risk factors of central nervous system (CNS) diseases, and clarify mechanisms of dichotomous injury outcomes between men and women. Microglia morphology, complement receptor 3 (CR3), and neuroinflammatory proteins were studied in the somatosensory cortex and hippocampus CA1 among male and female (estrus, diestrus and ovarian failure) mice (C67Bl/6J, 16 weeks) to discover relationships among microglia morphology, region, sex, and neuroinflammatory environment. The human post-menopause period was modeled in mice using 4-vinylcyclohexene diepoxide injections which induced accelerated ovarian failure. Using methods to quantify ramification, shape, and complexity, we discovered differences in microglia morphologies according to brain region and sex group. Microglia endpoints, process length, and complexity were increased in the female ovarian failure group when compared to other sex groups. Microglia were smaller and less complex in the hippocampus region versus the cortex. Microglia phagocytic receptor CR3 was assessed using immunohistochemistry methods and was increased in the female diestrus cortex when compared to male and females in estrus; no sex differences were observed in the hippocampus. Neuroinflammatory protein concentrations were screened using Multiplex Luminex methods and were detected in cortex homogenates, however, no differences among the sex groups were observed. Microglia morphology and CR3 are diverse in the adult healthy

cortex according to region, sex and ovarian function, indicative of diversity in microglial constitutive form and function. Such differences may be influenced by parenchymal context such as neuronal and glial populations/activity or differences in sex hormone concentrations, systemically circulating or *in situ*, rather than by concentrations of neuroinflammatory proteins. Understanding sex and region specific differences in the brain's surveillance and maintenance system will provide insight into the variability of patient risk and outcomes in CNS diseases.

Introduction

The importance of sex differences in brain neuropathology is highlighted by central nervous system (CNS) diseases that have a distinguished sex-specific prevalence. These include multiple sclerosis (Ramien et al., 2016), Alzheimer's (Li and Singh, 2014), Parkinson's disease (Kowal et al., 2013), an increased prevalence of anxiety, depressive disorders (Altemus et al., 2014) and CNS autoimmune diseases (Ngo et al., 2014) in females, as well as neurological injury with sex-specific dichotomous outcomes (i.e. ischemic stroke) (Mozaffarian et al., 2016). Microglia are best known and vigorously studied in their roles as the brain immune cell and first responder to diseases and brain injury (Davalos et al., 2005; Morrison and Filosa, 2016; Nimmerjahn et al., 2005; Tremblay et al., 2011). Pre–clinical animal models have shown that sex hormones have a potent effect on microglia mediated neuroplasticity (Hansberg-Pastor et al., 2015) and neuroinflammation (Hanamsagar and Bilbo, 2016; Villa et al., 2016) during development, health and disease. In the healthy brain, microglia are necessary to establish sex specific behaviors during growth and development (Lenz et al., 2013; Lenz and McCarthy, 2014; McCarthy et al., 2015) and are responsible for parenchymal surveillance and synaptic pruning (Siskova and Tremblay, 2013; Tremblay et al., 2011). As such, sex differences in microglia actions to maintain the adult brain during health are a component of observed sex differences in microglia responses to pathology and related functional outcomes.

In the healthy brain, microglia are observed as ramified cells with small somas (Kettenmann et al., 2011), however, with observable morphological distinctions among brain regions (Lawson et al., 1990), which have only begun to be assessed using quantitative methods (Fernandez-Arjona et al., 2017). A ramified cell is one that has a complicated network of processes that originate

from the cell soma. The highly ramified morphology reflects the dynamic microglia activity (process extension and retraction) necessary to continuously monitor their parenchymal domains during health. In fact, microglia process extension and retraction rates are estimated to be 1.47 µm/min in the healthy brain (Nimmerjahn et al., 2005), a rate necessary for complete brain assessment every few hours. Therefore, the historical functional categorization of ramified microglia as "resting" marginalizes their important contributions toward brain maintenance and homeostasis. Microglia are not merely responders to injury but have a significant role in neurological (Cunningham et al., 2013; Siskova and Tremblay, 2013) and behavioral development (Lenz et al., 2013) as well as maintaining neuronal networks in the adult brain (Ji et al., 2013; Wake et al., 2009) and working collaboratively with other glia (Domingues et al., 2016).

A growing body of evidence suggests that the nuances of microglia function in the healthy brain are a basis for neuropathology after injury, infection, and stressors (Hristovska and Pascual, 2015; Kierdorf and Prinz, 2013). Microglia's surveillance function is vital to maintain the complex neural network of glia, neurons, and vasculature. A disruption in this function from non-infectious origins (i.e. chronic stress) not only detracts from this important role but may promote a more injurious microglia phenotype (Bisht et al., 2016). Our study of microglia and biological variables (sex, cycle and ovarian function) in the healthy brain regions is a foundation to understanding sex differences in brain homeostasis, not only as an emerging field, but also as the inexorable antecedent to sex differences in neuropathology.

Because of their surveillance function, we suggest that both subtle and gross changes in

microglia morphologies serve as indicators of changed parenchymal surroundings. In order to capitalize on this potential, sensitive tools to precisely quantify microglia morphology (Karperien et al., 2013; Morrison and Filosa, 2013; Morrison and Filosa, 2016) have been employed here to distinguish the effects of sex, estrus cycle, and ovarian failure on microglia morphology in healthy brain regions. We examined the constitutive presence of complement receptor 3 (CR3) to gain insight into microglia phagocytic potential. Lastly, we screened for differences in inflammatory protein concentrations in the healthy brain. For additional comparison, two brain regions were included in the study that were previously shown to have high (hippocampus) or low (cortex) constitutive expression of estrogen receptors (Merchenthaler et al., 2004; Saito et al., 2016). In addition, both the cortex and hippocampus regions are relevant to a diversity of CNS injury models. The data presented in this manuscript provide an intricate characterization of microglia morphology, function and neuroinflammatory environment in healthy mice that varies according brain region, sex, estrus cycle, and ovarian function.

Methods

Animals and ovarian failure (OF) mouse model of post-menopause.

All animal handling and experiments were performed according to methods approved by and in compliance with the University of Arizona Institutional Animal Care and Use Committee and according to the National Institutes of Health guide for the care and use of Laboratory animals (#14-539). All animals were housed in rooms with a 12-hr light/dark schedule (7am-7pm). Male and female C57Bl6/J (15wk old) mice were purchased from Jackson Laboratories. Additional female C57Bl6/J mice were purchased at 5wk old in order to induce OF as a model of the human post-menopause period. We employed the OF protocol as previously published (Haas et al.,

2007; Van Kempen et al., 2014). Briefly, 5wk old female mice were injected for 21 days with 4-vinylcyclohexene diepoxide (VCD, 160 mg/kg/i.p./day). Follicle depletion and ovarian cessation was assessed ~65 days after first injection via vaginal lavage, and ovarian failure was confirmed by observing 15 days of persistent diestrus.

Brain tissue was then collected from all animals between ages 16wk and 18wk old between 10am and 12pm. In female mice, estrus cycle, or lacking cyclicity as in the case with female OF mice, was assessed via vaginal lavage (please see **Additional Figure 1**) and brain tissue was collected when either in diestrus, estrus or OF. All animals were sedated with 5% isofluorane delivered via a 20% oxygen/80% air mixture and systemically perfused with ice-cold phosphate buffered saline via cardiac puncture, after which brain tissue was immediately removed. Hemispheres were separated and were used for either immunohistochemistry (IHC; fixed) or for multiplex immunoassay (fresh frozen). For fixed tissue, the hemisphere was fixed for 24h in a 4% paraformaldehyde solution followed by 72h in a 30% sucrose solution, after which the tissue was dried and stored at -80°C until sectioning into coronal sections. The remaining hemisphere was rapidly frozen and stored at -80°C until sectioning and protein extraction.

Immunohistochemistry

All IHC was completed on one hemisphere of tissue. Each hemisphere was sectioned into 50µm coronal sections (Leica cryostat) and stored at -20°C in a cryoprotectant solution (50% 50mM PBS, 30% ethylene glycol, 20% glycerol) until IHC experiments. Our IHC protocol, similar to as previously published (Morrison and Filosa, 2013; Morrison and Filosa, 2016), results in double staining of microglia with anti-iba1 and CR3 (anti-CD18 and anti-CD11b). Free floating brain

sections were first blocked in 10% horse serum solution (0.01M PBS, 0.05% Triton, and 0.04% NaN_3) for 1h followed by a 72h incubation with primary antibodies as appropriate: rabbit anti-iba1 at 1:1000 (Wako, 019-19741), rat anti-ITAM/CD11b at 1:100 (ThermoFisher, RM2800) and rat anti-Integrin beta-2/CD18 at 1:100 (Millipore, MABT42). A 4-h incubation of 1:250 secondary primaries (Jackson ImmunoResearch Laboratories) followed: donkey anti-rabbit Alexa 488 (711-546-152); donkey anti-rat Alexa 594, (712-585-150). All tissue was incubated in solutions common to all groups to avoid group/batch differences. All reactions were carried forward at room temperature; washes between incubations were done with 0.01M PBS for 15min. Slices were then mounted onto slides using Vectashield (Vector Laboratories, H-1000). We incubated sections with secondary antibodies only to assess unspecific binding and detected none (**Additional Figure 2**).

Photomicrograph Acquisition and Analysis

Two regions were assessed for basal microglia morphology and presence of CR3 following IHC—the somatosensory cortex cortical layers II-IV and the hippocampus CA1 region (as depicted in **Figure 1A and 1B**). These regions were selected based on their relevance to injury models involving the somatosensory cortex (ischemic stroke and traumatic brain injury) as well as models used to study memory impairment (hippocampus CA1 region). In addition, both regions express estrogen receptors to a different extent (Merchenthaler et al., 2004; Saito et al., 2016). One photomicrograph was acquired in each region. Imaging was accomplished using either a Leica SP5-II confocal microscope for morphology analysis [30-µm Z-stack at 2-µm intervals, 40X/1.25Na PL- Apo oil objective, and a 387.5µm x 386.8µm imaged area (2696 pixels x 2691 pixels)] or a Zeiss 880 NLO for microglia CR3 assessment [30-µm Z-stack at 1-

µm intervals, 40X/1.3Na C PL-Apo oil objective, and a 212.6 µm x 212.6µm imaged area (1200 pixels x 1200 pixels)]. Photomicrographs were stacked and split using ImageJ plugins (National Institute of Health, https://imagej.nih.gov/ij/) in order to obtain maximum intensity projections of all channels. Photomicrographs, separated as channels, were saved as TIFF files prior to analysis and examples are shown in **Figure 1A** and **Figure 1B**. Microglia morphology and the location of CR3 was determined in male, diestrus female, estrus female and ovarian failure female mice using ImageJ plugins and detailed below.

Microglia Morphology

The extent of microglia ramified morphology was quantified using an objective and computer-aided skeleton analysis method as previously published in detail (Morrison and Filosa, 2013; Morrison and Filosa, 2016). Briefly, a series of ImageJ plugins (adjust brightness, unsharp mask, and despeckle) were consistently applied in order to ensure adequate process visualization before the conversion to binary and skeletonized images. The skeletonized representations of original photomicrographs were used for data collection. The AnalyzeSkeleton (2D/3D) plugin (developed and maintained by Arganda-Carreras et al. (Arganda-Carreras et al., 2010)) was used to tag elements of microglia skeletons as processes (orange slab voxels) and endpoints (blue) for data collection. We summarized the number of endpoints and process length from AnalyzeSkeleton (2D/3D) plugin data output and all data were divided by cell soma counts (Young and Morrison, 2018).

Fractal analysis

We measured microglia complexity of individual cells in addition to cell ramification which was

determined from entire photomicrograph fields. The plugin FracLac for ImageJ (Karperien, 1999-2013) was used to determine fractal dimension (complexity), lacunarity (heterogeneity), density (size) and span ratio (elongation) of microglia cells (Karperien et al., 2013; Karperien and Jelinek, 2015). Using a grid and random number generator, three microglia were randomly chosen from each photomicrograph that was also used for Skeleton Analysis. Individual microglia were first made binary through a similar process as described above. Additional structures that abut and surround each cell were manually excluded from the analysis using a Wacom tablet. Binary cells were then converted to outlines using ImageJ. Exemplars of this workflow process in each group are provided in **Figure 2A and 2B**. Fractal dimension (D_B) quantifies the level of detail of each cell's outline using a box counting protocol that determines change in pixel detail as magnification increases. For 2D cell outlines, fractal dimension values range from 1 to 2, where 1 is considered to be a simple circle. Lacunarity is a measure of the heterogeneity or variability of complex morphologies. To determine lacunarity, fractal dimension is assessed after the cell has been rotated multiple times (4) and the coefficient of variation (CV) is calculated. CV will be low for homogenously shaped cells and high for heterogeneously shaped cells. These calculations and relationships are best summarized in the reference guide provided for FracLac for Image J (https://imagej.nih.gov/ij/plugins/fraclac/FLHelp/BoxCounting.htm) and additional associated references (Karperien, 1999-2013; Karperien and Jelinek, 2015). Cell morphology data were averaged for each parameter to obtain a representative value for each animal (animal *n* is reported in figure).

Complement receptor 3 (CD18 and CD11b) analysis

Complement receptor 3 (CD18/CD11b) mean fluorescence intensity was determined from photomicrographs using Image J software and methods that have been previously published (Morrison and Filosa, 2013; Morrison and Filosa, 2016). Using consistent thresholding settings, positive staining for CD18 and CD11b were determined for all photomicrographs. Positive staining was determined on the basis of secondary only staining (**Additional Figure 2**) and microglia iba-1 counterstain. Mean fluorescence intensity values were recorded and normalized by the number of cells in each image.

Multiplex Luminex Immunoassay

Cortex was sectioned from frozen mouse hemispheres (n = 8-11 per group; see figure for exact sample sizes), homogenized in ice-cold lysis buffer buffer containing
20 mmol/L Tris-HCl (pH 7.5), 150 mmol/L NaCl, 1 mmol/L PMSF, 0.05% Tween® 20, and a cocktail of protease inhibitors and 1% of each: protease inhibitor cocktail (Sigma-Aldrich, Saint Louis, MO #P8340), 1 mmol/L PMSF (Sigma-Aldrich, P7626), and 200mM Na_3VO_4 (Sigma-Aldrich, S6508). Tissue homogenate was centrifuged following a 2-h digestion at 4°C and the supernatant was collected to determine protein concentration using the Bradford method; bovine serum albumin was used as the standard. Tissue lysate (0.75 mg/ml for all samples) was screened for the presence of 18 specific chemokines, cytokines, and growth factors and quantified by the Luminex Magpix (Austin, TX) using the high sensitivity immunoassay purchased from Millipore (Mouse cytokine magnetic 18-Plex Panel # MHSTCMAG-70K, Burlington, MA) according to the manufacturer's recommendations. Additional Table 1 lists all analytes screened for along with additional pertinent information (detectable range, quality control and response to positive control).

Statistical Analysis

All data are presented as mean ± standard error of mean (SEM). Sex and region differences were determined using a two-way ANOVA test with Sidak's post-hoc testing. Differences in concentrations of neuroinflammatory proteins were determined by a Kruskal-Wallis test with Dunn's multiple comparison where appropriate. All reported p values have been adjusted for multiple comparisons. GraphPad Prism 6 was used for statistical analyses. SigmaPlot was used to generate the 3D scatterplot. The datasets generated and/or analyzed during the current study are available from the corresponding author on reasonable requests

Results

Microglia ramification is different by region and sex in the healthy brain.

Our first aim was to examine sex and ovarian function differences in microglia ramified morphologies among healthy adult mice in the cortex and the hippocampus. Photomicrographs of microglia in the cortex and hippocampus at 40X magnification are shown in **Figure 1A and 1B**, respectively. Cropped photomicrographs are included to better illustrate the microglia morphology detail that was analyzed using the skeleton analysis method (Young and Morrison, 2018). The number of cell somas in each photomicrograph field was quantified in order to normalize subsequent skeleton analysis data. We determined that there were differences in cell counts/field according to sex group and region (two-way ANOVA region: $F_{(1,90)} = 45.92$, $p < 0.0001$; sex: $F_{(3,90)} = 8.78$, $p < 0.0001$; interaction: $F_{(3,90)} = 1.66$, $p = 0.18$). In the cortex, soma/field were significantly less in FOF mice when compared to all other groups while in the hippocampus, cell soma/field were increased in the female estrus group when compared to the

male and FOF group (**Figure 1C**). Next, we quantified the differences in microglia ramified morphology in the cortex and hippocampus according to sex, cycle and ovarian failure using two variables: microglia process length and number of endpoints per cell (**Figure 1D and 1E**). Microglia process length/cell was different by sex and region (two-way ANOVA: region: $F_{(1,90)} = 8.82$, $p = 0.003$; sex: $F_{(3,90)} = 28.02$, $p < 0.0001$; interaction: $F_{(3,90)} = 3.62$, $p = 0.02$). In the cortex, microglia process length/cell was greatest in the females with ovarian failure while in the hippocampus process length/cell was greatest in male and FOF groups when compared with females in estrus or diestrus (**Figure 1D**). Similarly, the number of process endpoints/cell was different by sex and region (two-way ANOVA: region: $F_{(1,90)} = 206.1$, $p < 0.0001$; sex: $F_{(3,90)} = 10.30$, $p < 0.0001$; interaction: $F_{(3,90)} = 3.76$, $p = 0.01$). In contrast to process length/cell data, sex differences in endponts/cell were present in the cortex but not hippocampus (**Figure 1E**). Although all microglia in the healthy cortex and hippocampus are ramified, our data show subtle morphologic differences according to region and sex.

Microglia shape, size and span are different by region or sex in the health brain.

We next examined cell complexity using fractal analysis made possible by FracLac for Image J (Karperien, 1999-2013). Fractal dimension, a FracLac data output, summarizes the complexity of a shape and is therefore well suited to detect subtle changes in microglia shapes that are in addition to cell ramification. Moreover, fractal analysis is carried out on individual microglia rather than the entire photomicrograph. An example of the data collection process, from image to individual microglia shape in the cortex and hippocampus data are shown in **Figure 2A and 2B**. Fractal dimension is calculated as a change pixel in detail as scale changes (please refer to the ImageJ manual (Karperien, 1999-2013) for a more comprehensive definition and equation);

Fractal dimension ranges from 1-2 for shape outlines. In this data set (cortex and hippocampus) fractal dimension ranged from 1.399 to 1.63 with the lowest value occurring in the cortex diestrus female group and highest in the hippocampus FOF group. Fractal dimension was different by region and sex (two-way ANOVA: region: $F_{(1,90)} = 231.4$, $p < 0.0001$; sex: $F_{(3,90)} = 17.63$, $p < 0.0001$; interaction: $F_{(3,90)} = 4.01$, $p = 0.01$). In the cortex, fractal dimension (cell complexity) was the highest in the FOF group while in the hippocampus, fractal dimension was high in both male and FOF groups (**Figure 2C**).

Lacunarity is a measure of cell heterogeneity. Lacunarity values are reported as a coefficient of variation (CV) and represent the variability of fractal dimension values returned as the same cell is rotated four times. If a cell has a low lacunarity then the CV value is low and therefore, the heterogeneity of the cell's shape is considered low, covering a proscribed space in a homogeneous manner. Cortex lacunarity was lower than hippocampus lacunarity (two-way ANOVA: region: $F_{(1,90)} = 171.4$, $p < 0.0001$; sex: $F_{(3,90)} = 1.77$, $p = 0.16$; interaction: $F_{(3,90)} = 4.16$, $p = 0.008$; **Figure 2D**).

Density is a measure of cell size and is calculated using the polygon that circumscribes the microglia shape: number of pixels of the shape outline ÷ polygon area (refer to ref 34 for detailed calculation information). Cell size was different between the hippocampus and cortex and without sex differences within each region (two-way ANOVA: region: $F_{(1,90)} = 31.87$, $p < 0.0001$; sex: $F_{(3,90)} = 2.56$, $p = 0.06$; interaction: $F_{(3,90)} = 0.11$, $p = 0.96$; **Figure 2E**).

Lastly, span ratio summarizes microglia elongation and is calculated as a ratio of cell length and

width. In this data set, span ratio was not different according to either region or sex (two-way ANOVA region: $F_{(1,90)} = 0.75$, $p = 0.39$; sex: $F_{(3,90)} = 0.53$, $p = 0.66$; interaction: $F_{(3,90)} = 2.85$, $p = 0.04$; **Figure 2F**).

Integrating skeleton and fractal analysis outcomes reveal subtle morphologic differences among ramified microglia.

We created a 3D plot of mean fractal dimension, process length/cell and density data for all groups and regions (**Figure 3**) while all data points are summarized in **Additional Figure 3**. These three variables were chosen to represent three different aspects of the morphology analysis (ramification, complexity, and cell size). Including additional variables would be redundant as process length/cell was significantly correlated to endpoints/cell ($r = 0.63$, $p < 0.0001$), fractal dimension ($r = 0.61$, $p < 0.0001$), lacunarity ($r = -.34$, $p = 0.02$), and density ($r = 0.3$, $p = 0.04$) but not span ratio ($r = 0.-24$, $p = 0.12$). Fractal dimension was significantly correlated to process length/cell ($r = 0.61$, $p < 0.0001$), lacunarity ($r = -0.76$, $p < 0.0001$), density ($r = 0.85$, $p < 0.0002$), and span ratio ($r = -0.35$, $p = 0.02$) but not endpoints/cell ($r = 0.2$, $p = 0.18$). When the mean data for the three morphology variables are plotted we observe that microglia morphology in the CA1 hippocampus region is distinct from that of the somatosensory cortex region. In addition, microglia morphology in the FOF group yield the largest values in both regions. These result are descriptive of subtle differences in the extent of microglia complexity, ramification and size according to sex and region.

Constitutive presence of microglia CR3 in the healthy brain among male and female mice.

The CR3 receptor is formed by integrin alpha and beta subunits CD11b and CD18. The

constitutive presence of CR3 on microglia was assessed to determine sex differences in complement related physiology such as phagocytosis. Example photomicrographs of CR3 immunohistochemistry in each group and region are shown in **Figures 4A and 4B** with a single cropped cell to illustrate co-localization of CR3 to microglia (iba1). **Figure 4C** summarizes the means ± SEM and statistical analysis of microglia soma number in groups and regions. We determined that there were differences in cell counts/field according to sex group and region (two-way ANOVA region: $F_{(1,72)} = 12.89$, $p = 0.0006$; sex: $F_{(3,72)} = 4.74$, $p = 0.005$; interaction: $F_{(3,72)} = 0.29$, $p = 0.83$). In the cortex, soma/field was less in FOF mice when compared to female diestrus ($p = 0.05$). Next, we report differences in the percent area of CR3 per cell according to group and region in **Figure 4D** (two-way ANOVA region: $F_{(1,72)} = 4.33$, $p = 0.04$; sex: $F_{(3,72)} = 3.76$, $p = 0.01$; interaction: $F_{(3,72)} = 5.02$, $p = 0.003$). In the cortex, the area of CR3 is increased in female diestrus ($n = 10$) mice versus female estrus and males ($p = 0.005$, $n = 10$ and $p < 0.0001$, $n = 10$, respectively) whereas there were no sex differences in the hippocampus.

Constitutive cortical neuroinflammatory protein concentrations are similar among male and female mice.

To complement microglia anatomy and physiology in the healthy brain, we screened for the presence of detectable neuroinflammatory proteins in the cortex among male and female (diestrus, estrus and OF) mice using a Multiplex Luminex assay. **Figure 5A** we illustrate the brain region sampled for this screening. **Additional Table 1** lists all analytes assessed, the detectable ranges for the commercial assay, the quality controls used to validate assay accuracy, and the response to a positive control. The following analytes were not reported due an inability to detect analyte within given assay range for each sample (GM-CSF, INFγ, IL5, IL6, IL7, IL10,

IL12, IL17a, MCP1, and TNFα). Analytes IL4, IL13, and IL17α failed to respond to the positive control and were excluded from analysis. The mean ± SEM and statistical analysis of the remaining 6 out of 18 analytes are reported in **Figure 5B**: IL1α, IL1β, IL2, LIX, KC/IL8 and MIP2. Although a sample size of 10 was used for data collection, low bead counts limited data analysis in some samples reducing sample size further and the actual sample sizes are shown in Figure 5B. A non-parametric Kruskal-Wallis was used to test for differences among groups for all analytes. IL1α: $H = 3.92$, 3df, $p = 0.27$; IL1β: $H = 7.55$, 3df, $p = 0.05$; IL2: $H = 5.9$, 3df, $p = 0.12$; LIX: $H = 2.01$, 3df, $p = 0.57$; KC/IL8: $H = 3.75$, 3df, $p = 0.29$; MIP2: $H = 4.39$, 3df, $p = 0.22$. In summary, IL1β was the only analyte screened to demonstrate a small difference among groups with the lowest concentration present in female estrus cortex versus female diestrus ($p = 0.06$).

Discussion

Microglia are constitutively active in the healthy brain in their functions to surveil the parenchyma, maintain glial and neuronal homeostasis, and to detect and ameliorate brain pathology. They accomplish these functions via constant communication with neurons and glia (Bianchi et al., 2010; Fontainhas et al., 2011; Gyoneva et al., 2009; Orr et al., 2009; Saijo and Glass, 2011). Changes in neuronal and glial functions are immediately reflected by a change in microglia morphology observed as increased or decreased cell ramification, changed process polarity, and increased process movement (Davalos et al., 2005; Fontainhas et al., 2011; Nimmerjahn et al., 2005). Microglia morphologic transformations into polarized or amoeboid cells are well documented after robust brain injury (Morrison and Filosa, 2013; Ziebell et al., 2012). However, the more subtle differences in microglia morphology and the

neuroinflammatory milieu in the healthy brain according to brain region and sex have not been well studied. On this basis, our purpose was to investigate the differences in microglia morphology and CR3 in the healthy cortex and hippocampus among male and female mice. In addition, we investigated sex differences in neuroinflammatory protein concentrations in the healthy cortex. We found that, as expected, all cells were highly ramified in the healthy brain. Yet, we report that the morphometrics of these cells are distinctly different according to region and, for some measures, according to sex and ovarian function. In addition, the constitutive presence of CR3 on microglia was consistently increased in the female diestrus cortex when compared to the other sex groups while no sex differences were detected in the hippocampus. Lastly, of the six inflammatory proteins with detectable concentrations in the cortex, there were no discernable differences among groups.

Progesterone, 17β-estradiol, and testosterone are biologically active sex hormones that are reported to have corresponding receptors on brain cells (Mitterling et al., 2010). Sex hormones are lipid soluble; therefore, ligand/receptor interactions result in rapid effects via signaling cascades and long-term effects via transcriptional changes. The female estrus cycle has four phases that occur in a particular order (estrus, metaestrus, diestrus, and proestrus). The relative serum sex hormone concentrations (Nilsson et al., 2015) and sex hormone receptors fluctuate according to cycle phase (Mitterling et al., 2010) and vary between brain locations (Kato et al., 2013; Saito et al., 2016). The cessation of ovarian function, cyclic release of sex hormones, and termination of menses are among the elements that define the post-menopause phase of life for women. To model this phenomenon in mice, we employed the accelerated ovarian failure model (Haas et al., 2007) in which the occupational chemical VCD specificity targets primordial and

primary follicles via inhibited autophosphorylation of c-kit (Mark-Kappeler et al., 2011) to accelerate follicular atresia (Lee et al., 2017). This process occurs without detectable systemic pathology (Frye et al., 2012; Wright et al., 2008) and is summarized nicely by recent reviews (see (Brooks, Pollow, & Hoyer, 2016) and (Van Kempen, Milner, & Waters, 2011). In contrast to the ovariectomized mice, the accelerated ovarian model includes a "perimenopause" period in which ovarian hormone production and cyclicity is variable and declining. In mice, this period may last between 17 and 90 days and is therefore shorter (as a percentage of lifespan) when compared to humans (Brooks et al., 2016). However, a benefit of the accelerated ovarian failure model is that the "perimenopause" and ovarian failure status is inducible in young mice, therefore excluding the confounding variable of age (Brooks et al., 2016). As has been previously demonstrated, the three week VCD treatment protocol (160 mg/kg/i.p./day), employed in this study, did not elicit a neuroimmune response when compared to a positive control, either immediately following treatment or at a later time point (Van Kempen et al., 2014).

Microglia are capable of a broad range of ramified morphologies in the healthy brain (Lawson et al., 1990) and are highly responsive to neuronal activity via purines (Davalos et al., 2005; Koizumi et al., 2013; Nimmerjahn et al., 2005), neurotransmitters (Fontainhas et al., 2011), and chemokines (Saijo and Glass, 2011) . In fact, microglia "reach out" to survey neuronal synapses once per hour, a frequency that depends on neuronal activity (Wake et al., 2009). Microglia ramified morphologies and dynamic process movement are modified by transient or sustained changes in endogenous inotropic glutamatergic transmission (Fontainhas et al., 2011). Estrogens are known to rapidly modulate neuronal activity in the cortex and hippocampus. In the cortex,

estrogen potentiates excitatory synapses via increased sensitivity to glutamate through multiple mechanisms which include altered cellular responsiveness to inotropic glutamate receptor activation, opioid, dopamine, and GABA receptors (reviewed here (Kelly and Ronnekleiv, 2009; Malyala et al., 2005; Sellers et al., 2015)) as well as more long term effects by regulation of the brain transcriptome (Duclot and Kabbaj, 2015). Studied extensively in the hippocampus, estradiol increases sensitivity to glutamate or related receptors in both males and females, albeit by differing mechanisms (Oberlander and Woolley, 2016). Although much less studied, the presence of progesterone is correlated with increased neuronal spine density (Kato et al., 2013; Sanchez et al., 2013). On this basis, we suggest that differing microglia morphologies may be indicators of subtle differences in neuronal activity, influenced by an ebb-and-flow of sex hormone concentrations.

Our findings are suggestive of distinct morphologic differences between brain regions in the cortex and hippocampus. Regarding sex differences, a majority of morphologic differences exist between males and cycling females (regardless of cycle phase) or cycling females and OF females with few differences observed between diestrus and estrus females. A few scenarios could explain the similarity between estrus and diestrus females. First, it is possible that microglia morphology is similar among estrus cycle phases in the cycling female mouse due to the short duration with some phases lasting less than 24hours. Whether microglia morphology would differ according to cycle phase in humans, whom have a longer estrus cycle and longer phases, remains to be investigated. Second, animals were stratified into either diestrus and estrus female groups following vaginal lavage to determine cyclicity rather than according to a tissue or plasma sex hormone profile. Vaginal lavage assessment of cyclicity may not appropriately

approximate systemic or parenchymal sex hormone concentrations and therefore the diestrus and estrus females groups in this study may have similar sex hormone profiles. Third, it is unclear if microglia morphology is predominantly influenced by parenchymal versus systemic sex hormone concentrations. Studied previously in the hippocampus, tissue and plasma concentrations did vary with cycle phase. However, hippocampus concentrations of estrogen was reported to be 2-60 times greater than plasma concentrations (Kato et al., 2013). These data illuminate the importance of sex steroid concentrations in the tissue as well as the more often considered, systemic concentrations. Interestingly, while absent in male plasma, estradiol in the hippocampus was recorded as 2 fold greater than that of proestrus females (female groups reported to have the highest estradiol concentrations) and ~8 fold greater than ovariectomized rats (females with the lowest estradiol concentration) (Kato et al., 2013). Unfortunately, information of tissue sex steroid concentrations in specific brain regions other than the hippocampus is limited.

We used fractal analysis as an additional tool to assess microglia morphologies. Fractal analysis has been widely used as a morphometric analysis tool (Barreto et al., 2014; Fernandez-Arjona et al., 2017; Karperien et al., 2013; Karperien and Jelinek, 2015; Namjoshi et al., 2014; Orlowski et al., 2003; Soltys et al., 2001; Soltys et al., 2005) and added as a plugin to ImageJ for convenient use (Karperien, 1999-2013). In contrast with the skeleton analysis, fractal analysis is carried out on single cell and is therefore complementary to skeleton analysis. Although microglia processes are highly dynamic, the analysis of static morphologies summarizes the propensity of cells to have discernable characteristics according to distinct anatomical and physiologic differences within specific brain regions and diverse conditions. In addition to fractal dimension

(complexity), we report on the lacunarity, density, and span ratio of microglia shapes according to sex, cycle, and ovarian failure. Cells with higher lacunarity have a more heterogeneous shape and greater variability in how gaps are distributed within a shape (Barreto et al., 2014; Karperien and Jelinek, 2015). In our study, microglia shapes in the hippocampus had a higher lacunarity than microglia in the cortex, illustrating differences in how these cells occupy space for surveillance and homeostasis functions. We reveal a subtle clustering between region and sex by plotting skeleton data (process length/cell), complexity (fractal dimension), and cell size (density). In general, microglia in the hippocampus were smaller, but more ramified and complex in their morphology when compared to the cortex. Within each region, microglia in the female OF were the most ramified, complex, and occupying the largest area. We suggest that the observed increase in cell ramification in OF cortex is a morphologic response, or compensation, to decreased cell counts and serves a purpose to leave no brain parenchyma “un-touched” by their assessing processes. On the other hand, the increased cell complexity and ramification is likely independent of neuroinflammatory proteins (i.e. cytokines and chemokines) as these concentrations were similar among sex groups. It is possible that this change in morphology may contribute to an ineffective response to CNS challenge, accounting for worse outcomes following neuronal perturbation. Such a possibility needs further investigation and we demonstrate that it is possible to quantify microglia morphology during health or pathologic challenges that are both subtle (i.e. stress) and unsubtle (i.e. injury).

In addition to microglia morphology, we examined the presence of CR3, the first convergence of the classical and lectin pathways and initiation point of the alternative pathway. The CR3 ligands that are important to brain physiology/pathophysiology include lipopolysaccharide [LPS,

(Wright and Jong, 1986)], C3b/iC3b (Beller et al., 1982), fibrinogen (Wright et al., 1988), and high mobility group box protein 1 (HMGB-1). CR3-ligand interactions initiate cell chemotaxis or phagocytosis, and complement-mediated phagocytosis is a key component of brain development and adult physiology (Schafer et al., 2013). In the adult healthy brain, synaptic pruning is proposed via C3b-opsoinized synapses (Stevens et al., 2007; Tremblay et al., 2011) as neuronal and synaptic activity changes—a phenomenon that may disproportionally occur according to sex and estrus cycle (Crain and Watters, 2010). We observed that CR3 (CD11b/CD18) IHC resulted in consistently greater area of staining in the cortex of female diestrus mice. Increased CR3 correspond with less ramified or complex cells also observed in female diestrus mice. Unfortunately, our attempts to verify IHC data with western blot methods were unsuccessful likely because CD18 and CD11b is a complex-specific epitope. In addition, our attempts to investigate a diversity of phagocytic markers in the healthy brain (i.e. CD68, CD36, LAMP1 and RAB1) were also unsuccessful perhaps due to the absence of a pathologic condition. We speculate that the observed differences in microglia CR3 are the result of fluctuating sex hormone concentrations present in the parenchyma. Either the high CR3 is reflective of the female diestrus hormone milieu or remnant from the previous cycle phase (estrus). Interestingly, that microglia CR3 is different between cycling female mice (estrus versus diestrus) but remains consistently low in female OF and male mice indicates a plasticity in cortical microglia function or potential function that is lost in males and female OF mice. This difference may have a role in sex and ovarian function-related changes in microglia surveillance and homeostasis functions. In the hippocampus, microglia CR3 was relatively consistent among groups when compared to the diversity observed in the cortex. This finding is likely a reflection of different neuronal functions, sex hormone concentrations, or sex hormone receptors between

the two regions. These possibilities warrant additional investigations to more fully understand brain physiology.

Neuroinflammatory proteins (cytokines and chemokines) are hypothesized to have an influential role in determining microglia phagocytosis phenotypes that can contribute to either continued health or chronic disease (Amantea, 2016; Sokolowski and Mandell, 2011). We observed that inflammatory proteins are present and detectable in the healthy cortex, however, the concentration of these proteins were similar among sex groups in adult mice. Similarly, a previous investigation determined that mRNA levels of VEGF, arginase, and IL10 measured from primary microglia collected from 4 month old male mice were similar between males and females (Crain et al., 2013). Based on these data, we surmise that neuroinflammatory protein concentrations have a minimal influence on observed differences in microglia morphology and CR3 in the cortex. Although high sensitivity assays were used as a screening tool in this study, it is possible that current technologies have limited sensitivity to assess and detect small differences that may have a physiologic influence on microglia.

In conclusion, there are a number of neurodegenerative diseases with sex specific prevalence, and addressing and abating an individual's risk prior to the onset of illness is one of the hallmarks of preventative medicine. Investigating sex differences in the healthy brain is an important step towards more comprehensive healthcare, and understanding the brain's own surveillance and maintenance system may provide significant insight into the variability of patient outcomes in CNS diseases. We show differences in microglia morphology and CR3 receptor according to brain region and sex, estrus cycle and ovarian function. That

concentrations of neuroinflammatory proteins screened in this study were similar among the sexes, rule out associations between microglia morphology and inflammatory milieu in the healthy cortex. Whether our observations of morphologic differences are an indicator of sex-based differences in neuronal activities or a sex-specific physical attribute of microglia function have yet to be fully appreciated and are therefore worthy of further study.

Authors' Contributions

KY administered VCD injections, completed all image and data analysis (skeleton, fractal and CR3) and provided significant manuscript editing. Janet R contributed to statistical analyses and manuscript editing. Jenna R, SC, and AP completed tissue sectioning and assisted in skeleton analysis. HM conceived of and managed the project, completed IHC methods, confocal imaging, and wrote the manuscript. All authors read and approved the final manuscript.

Funding

This research was made possible by the University of Arizona College of Nursing (HM, KY) and Environmental Health Sciences-Transformative Research Undergraduate Experience with funding from the National Institute of Environmental Health Sciences R25-ES025494 (SC, AP).

Acknowledgements

Photomicrograph acquisition was made possible, in part, by funds from National Cancer Institute of the National Institutes of Health under award number P30 CA023074 (Leica Sp5-II) . Marley Facility housing the Zeiss 880 NLO is supported by the office of Research, Discovery and Innovation at the University of Arizona and partially funded through Arizona Proposition 301:

Technology and Research Initiative Fund (A.R.S.§15-1648). In addition, thank you to the University of Arizona Microscopy Alliance, Patricia Jansma and Douglas Cromey for their support and expertise.

Conflict of Interest

None

Figure Legends

Figure 1. Sex and regional differences in microglia ramified morphologies in the primary somatosensory cortex and hippocampus among healthy mice according to sex, cycle and ovarian function. A) Depiction of the primary somatosensory cortex (S1) brain layer 2/3 region imaged for all groups and representative maximum intensity 2D photomicrographs of anti-Iba1 immunohistochemistry identifying microglia soma and processes. Cropped images are below to provide detail. Sample sizes for cortex analysis are: male (M) n = 10, female diestrus (FD) n = 15, female estrus (FE) n = 9, female ovarian failure (FOF) n = 19. **(B)** Depiction of the hippocampus CA1 region imaged for all groups, representative maximum intensity 2D photomicrographs for each group with cropped images provided below. All quantitative skeleton analysis was carried out on full sized photomicrographs. Sample sizes for hippocampus analysis are: (M) n = 10, (FD) n = 12, (FE) n = 9, (FOF) n = 14. All scale bars = 10µm. Summarized data (mean and SEM) and statistical analysis (two-way ANOVA) of the number of microglia cell

somas/field **(C)** microglia processes length/cell **(D)** microglia process endpoints/cell **(E)** among male and female groups. All within region post-hoc comparisons and adjusted p values are reported in the figure.

Figure 2. Microglia complexity and size in the cortex of healthy male and female mice. A) Example of photomicrographs from the primary somatosensory cortex, individual cells (cropped), binary, and outlined cells in each group that was used for fractal analysis. Three cells were randomly chosen for fractal analysis from each photomicrograph and averaged. Animal N: male (M) n = 10, female diestrus (FD) n = 15, female estrus (FE) n = 9, female ovarian failure (FOF) n = 19. **(B)** Example of photomicrographs from the hippocampus, individual cells (cropped), binary, and outlined cells in each group that used for fractal analysis. Animal N: (M) n = 10, (FD) n = 12, (FE) n = 9, (FOF) n = 14. Summary data (mean and SEM) and statistical analysis (two-way ANOVA) of fractal dimension **(C)**, lacunarity **(D)**, density **(E)**, and span ratio **(F)**. All within region post-hoc comparisons and adjusted p values are reported in the figure.

Figure 3. A diversity of microglia morphologies in the cortex and hippocampus of healthy male and female mice. Mean fractal dimension, process length/cell and density morphology data were used to summarize differences in microglia morphology between brain regions and sex groups. Microglia size is consistently increased in the somatosensory cortex versus the hippocampus whereas microglia ramification and complexity are consistently increased in female ovarian failure mice when compared to the other sex groups.

Figure 4. Microglia CR3 healthy male and female mice. Example photomicrographs of CR3 in the cortex **(A)** and hippocampus **(B)** are illustrated with cropped images of microglia (iba1) alongside CR3 to show the specificity of CR3 to microglia. Sample sizes are male n = 10, female diestrus (FD) n = 10, female estrus n = 10, female ovarian failure n = 10 for both the cortex and hippocampus. Summarized data (mean and SEM) and statistical analysis (two-way ANOVA) of the number of microglia cell somas/field **(C)** and the percent area of CR3 positive staining per cell **(D)** among male and female groups in the cortex and hippocampus. All within region post-hoc analyses are reported in the figure and all scale bars = 10µm.

Figure 5. Neuroinflammatory protein concentrations in the cortex of male and female mice. **A)** An illustration of the region (grey) sectioned from fresh frozen tissue for assessment of inflammatory protein concentrations using Multiplex methods. **B)** Summary data (mean and SEM) and statistical analysis (Kruskal-Wallis) of analyzed and reportable analytes. Sample size applied to the multiplex method for each group were: male n = 10, female diestrus n = 9, female estrus n = 10, post-menopause female n = 15. Data were not returned for all samples therefore the sample sizes used for statistical analysis are reported in the figure.

Additional Figure 1. Vaginal lavage of mice in estrus, diestrus and ovarian failure.

Additional Figure 2. Assessment for unspecific secondary binding.

IHC was carried out using an identical protocol and omitting the primary antibody. Tissue was imaged to assess unspecific immunofluorescence on the Leica or Zeiss microscope.

Additional Figure 3. 3D plot of all fractal dimension, process length/cell and density morphology data.

Additional Table 1. Multiplex analysis additional information. Columns listing all analytes screened using the commercial assay (mouse cytokine magnetic 18-Plex Panel # MHSTCMAG-70K, Burlington, MA), detectable range of the standard curve for each analyte, quality controls (plate controls), and the assay (mean concentration ± SEM) response to an experimental positive control, brain injury. The number of animals used for the experimental control was n = 27. The number of experimental control animals with returned values for each analyte are listed in the final column.

PeerJ Preprints | https://doi.org/10.7287/peerj.preprints.26937v1 | CC BY 4.0 Open Access | rec: 16 May 2018, publ: 16 May 2018

Altemus, M., Sarvaiya, N., Neill Epperson, C., 2014. Sex differences in anxiety and depression clinical perspectives. Front Neuroendocrinol. 35**,** 320-30.

Amantea, D., 2016. Polarizing the immune system towards neuroprotection in brain ischemia. Neural Regen Res. 11**,** 81-2.

Arganda-Carreras, I., Fernandez-Gonzalez, R., Munoz-Barrutia, A., Ortiz-De-Solorzano, C., 2010. 3D reconstruction of histological sections: Application to mammary gland tissue. Microsc Res Tech. 73**,** 1019-29.

Barreto, G.E., Santos-Galindo, M., Garcia-Segura, L.M., 2014. Selective estrogen receptor modulators regulate reactive microglia after penetrating brain injury. Front Aging Neurosci. 6**,** 132.

Beller, D.I., Springer, T.A., Schreiber, R.D., 1982. Anti-Mac-1 selectively inhibits the mouse and human type three complement receptor. J Exp Med. 156**,** 1000-9.

Bianchi, R., Giambanco, I., Donato, R., 2010. S100B/RAGE-dependent activation of microglia via NF-kappaB and AP-1 Co-regulation of COX-2 expression by S100B, IL-1beta and TNF-alpha. Neurobiol Aging. 31**,** 665-77.

Bisht, K., Sharma, K.P., Lecours, C., Sanchez, M.G., El Hajj, H., Milior, G., Olmos-Alonso, A., Gomez-Nicola, D., Luheshi, G., Vallieres, L., Branchi, I., Maggi, L., Limatola, C., Butovsky, O., Tremblay, M.E., 2016. Dark microglia: A new phenotype predominantly associated with pathological states. Glia. 64**,** 826-39.

Brooks, H.L., Pollow, D.P., Hoyer, P.B., 2016. The VCD Mouse Model of Menopause and Perimenopause for the Study of Sex Differences in Cardiovascular Disease and the Metabolic Syndrome. Physiology (Bethesda). 31**,** 250-7.

Crain, J.M., Watters, J.J., 2010. Estrogen and P2 Purinergic Receptor Systems in Microglia: Therapeutic Targets for Neuroprotection. Open Drug Discov J. 2**,** 148-167.

Crain, J.M., Nikodemova, M., Watters, J.J., 2013. Microglia express distinct M1 and M2 phenotypic markers in the postnatal and adult central nervous system in male and female mice. J Neurosci Res. 91**,** 1143-51.

Cunningham, C.L., Martinez-Cerdeno, V., Noctor, S.C., 2013. Microglia regulate the number of neural precursor cells in the developing cerebral cortex. J Neurosci. 33**,** 4216-33.

Davalos, D., Grutzendler, J., Yang, G., Kim, J.V., Zuo, Y., Jung, S., Littman, D.R., Dustin, M.L., Gan, W.B., 2005. ATP mediates rapid microglial response to local brain injury in vivo. In Nat Neurosci. Vol. 8, ed.^eds., United States, pp. 752-8.

Domingues, H.S., Portugal, C.C., Socodato, R., Relvas, J.B., 2016. Oligodendrocyte, Astrocyte, and Microglia Crosstalk in Myelin Development, Damage, and Repair. Front Cell Dev Biol. 4**,** 71.

Duclot, F., Kabbaj, M., 2015. The estrous cycle surpasses sex differences in regulating the transcriptome in the rat medial prefrontal cortex and reveals an underlying role of early growth response 1. Genome Biol. 16**,** 256.

Fernandez-Arjona, M.D.M., Grondona, J.M., Granados-Duran, P., Fernandez-Llebrez, P., Lopez-Avalos, M.D., 2017. Microglia Morphological Categorization in a Rat Model of Neuroinflammation by Hierarchical Cluster and Principal Components Analysis. Front Cell Neurosci. 11**,** 235.

Fontainhas, A.M., Wang, M., Liang, K.J., Chen, S., Mettu, P., Damani, M., Fariss, R.N., Li, W., Wong, W.T., 2011. Microglial morphology and dynamic behavior is regulated by ionotropic glutamatergic and GABAergic neurotransmission. PLoS One. 6**,** e15973.

Frye, J.B., Lukefahr, A.L., Wright, L.E., Marion, S.L., Hoyer, P.B., Funk, J.L., 2012. Modeling perimenopause in Sprague-Dawley rats by chemical manipulation of the transition to ovarian failure. Comp Med. 62**,** 193-202.

Gyoneva, S., Orr, A.G., Traynelis, S.F., 2009. Differential regulation of microglial motility by ATP/ADP and adenosine. In Parkinsonism Relat Disord. Vol. 15 Suppl 3, ed.^eds., England, pp. S195-9.

Haas, J.R., Christian, P.J., Hoyer, P.B., 2007. Effects of impending ovarian failure induced by 4-vinylcyclohexene diepoxide on fertility in C57BL/6 female mice. Comp Med. 57**,** 443-9.

Hanamsagar, R., Bilbo, S.D., 2016. Sex differences in neurodevelopmental and neurodegenerative disorders: Focus on microglial function and neuroinflammation during development. J Steroid Biochem Mol Biol. 160**,** 127-33.

Hansberg-Pastor, V., Gonzalez-Arenas, A., Pina-Medina, A.G., Camacho-Arroyo, I., 2015. Sex Hormones Regulate Cytoskeletal Proteins Involved in Brain Plasticity. Front Psychiatry. 6**,** 165.

Hristovska, I., Pascual, O., 2015. Deciphering Resting Microglial Morphology and Process Motility from a Synaptic Prospect. Front Integr Neurosci. 9**,** 73.

Ji, K., Akgul, G., Wollmuth, L.P., Tsirka, S.E., 2013. Microglia actively regulate the number of functional synapses. PLoS One. 8**,** e56293.

Karperien, A., 1999-2013. FracLac for ImageJ. http://rsb.info.nih.gov/ij/plugins/fraclac/FLHelp/Introduction.htm . Vol., ed.^eds.

Karperien, A., Ahammer, H., Jelinek, H.F., 2013. Quantitating the subtleties of microglial morphology with fractal analysis. Front Cell Neurosci. 7.

Karperien, A.L., Jelinek, H.F., 2015. Fractal, Multifractal, and Lacunarity Analysis of Microglia in Tissue Engineering. Front Bioeng Biotechnol. 3.

Kato, A., Hojo, Y., Higo, S., Komatsuzaki, Y., Murakami, G., Yoshino, H., Uebayashi, M., Kawato, S., 2013. Female hippocampal estrogens have a significant correlation with cyclic fluctuation of hippocampal spines. Front Neural Circuits. 7**,** 149.

Kelly, M.J., Ronnekleiv, O.K., 2009. Control of CNS neuronal excitability by estrogens via membrane-initiated signaling. Mol Cell Endocrinol. 308**,** 17-25.

Kettenmann, H., Hanisch, U.K., Noda, M., Verkhratsky, A., 2011. Physiology of microglia. Physiol Rev. 91**,** 461-553.

Kierdorf, K., Prinz, M., 2013. Factors regulating microglia activation. Front Cell Neurosci. 7**,** 44.

Koizumi, S., Ohsawa, K., Inoue, K., Kohsaka, S., 2013. Purinergic receptors in microglia: functional modal shifts of microglia mediated by P2 and P1 receptors. Glia. 61**,** 47-54.

Kowal, S.L., Dall, T.M., Chakrabarti, R., Storm, M.V., Jain, A., 2013. The current and projected economic burden of Parkinson's disease in the United States. Mov Disord. 28**,** 311-8.

Lawson, L.J., Perry, V.H., Dri, P., Gordon, S., 1990. Heterogeneity in the distribution and morphology of microglia in the normal adult mouse brain. Neuroscience. 39**,** 151-70.

Lee, J.H., Lee, M., Ahn, C., Kang, H.Y., Tran, D.N., Jeung, E.B., 2017. Parabens Accelerate Ovarian Dysfunction in a 4-Vinylcyclohexene Diepoxide-Induced Ovarian Failure Model. Int J Environ Res Public Health. 14.

Lenz, K.M., Nugent, B.M., Haliyur, R., McCarthy, M.M., 2013. Microglia are essential to masculinization of brain and behavior. In J Neurosci. Vol. 33, ed.^eds., United States, pp. 2761-72.

Lenz, K.M., McCarthy, M.M., 2014. A Starring Role for Microglia in Brain Sex Differences. Neuroscientist.

Li, R., Singh, M., 2014. Sex differences in cognitive impairment and Alzheimer's disease. Front Neuroendocrinol. 35**,** 385-403.

Malyala, A., Kelly, M.J., Ronnekleiv, O.K., 2005. Estrogen modulation of hypothalamic neurons: activation of multiple signaling pathways and gene expression changes. Steroids. 70**,** 397-406.

Mark-Kappeler, C.J., Sen, N., Lukefahr, A., McKee, L., Sipes, I.G., Konhilas, J., Hoyer, P.B., 2011. Inhibition of ovarian KIT phosphorylation by the ovotoxicant 4-vinylcyclohexene diepoxide in rats. Biol Reprod. 85**,** 755-62.

McCarthy, M.M., Pickett, L.A., VanRyzin, J.W., Kight, K.E., 2015. Surprising Origins of Sex Differences in the Brain. Horm Behav.

Merchenthaler, I., Lane, M.V., Numan, S., Dellovade, T.L., 2004. Distribution of estrogen receptor alpha and beta in the mouse central nervous system: in vivo autoradiographic and immunocytochemical analyses. J Comp Neurol. 473**,** 270-91.

Mitterling, K.L., Spencer, J.L., Dziedzic, N., Shenoy, S., McCarthy, K., Waters, E.M., McEwen, B.S., Milner, T.A., 2010. Cellular and subcellular localization of estrogen and progestin receptor immunoreactivities in the mouse hippocampus. J Comp Neurol. 518**,** 2729-43.

Morrison, H.W., Filosa, J.A., 2013. A quantitative spatiotemporal analysis of microglia morphology during ischemic stroke and reperfusion. In J Neuroinflammation. Vol. 10, ed.^eds., pp. 4.

Morrison, H.W., Filosa, J.A., 2016. Sex differences in astrocyte and microglia responses immediately following middle cerebral artery occlusion in adult mice. Neuroscience.

Mozaffarian, D., Benjamin, E.J., Go, A.S., Arnett, D.K., Blaha, M.J., Cushman, M., Das, S.R., de Ferranti, S., Despres, J.P., Fullerton, H.J., Howard, V.J., Huffman, M.D., Isasi, C.R., Jimenez, M.C., Judd, S.E., Kissela, B.M., Lichtman, J.H., Lisabeth, L.D., Liu, S., Mackey, R.H., Magid, D.J., McGuire, D.K., Mohler, E.R., 3rd, Moy, C.S., Muntner, P., Mussolino, M.E., Nasir, K., Neumar, R.W., Nichol, G., Palaniappan, L., Pandey, D.K., Reeves, M.J., Rodriguez, C.J., Rosamond, W., Sorlie, P.D., Stein, J., Towfighi, A., Turan, T.N., Virani, S.S., Woo, D., Yeh, R.W., Turner, M.B., 2016. Executive Summary: Heart Disease and Stroke Statistics-2016 Update: A Report From the American Heart Association. Circulation. 133**,** 447-54.

Namjoshi, D.R., Cheng, W.H., McInnes, K.A., Martens, K.M., Carr, M., Wilkinson, A., Fan, J., Robert, J., Hayat, A., Cripton, P.A., Wellington, C.L., 2014. Merging pathology with biomechanics using CHIMERA (Closed-Head Impact Model of Engineered Rotational Acceleration): a novel, surgery-free model of traumatic brain injury. Mol Neurodegener. 9**,** 55.

Ngo, S.T., Steyn, F.J., McCombe, P.A., 2014. Gender differences in autoimmune disease. Front Neuroendocrinol. 35**,** 347-69.

Nilsson, M.E., Vandenput, L., Tivesten, A., Norlen, A.K., Lagerquist, M.K., Windahl, S.H., Borjesson, A.E., Farman, H.H., Poutanen, M., Benrick, A., Maliqueo, M., Stener-Victorin, E., Ryberg, H., Ohlsson, C., 2015. Measurement of a Comprehensive Sex Steroid Profile in Rodent Serum by High-Sensitive Gas Chromatography-Tandem Mass Spectrometry. Endocrinology. 156**,** 2492-502.

Nimmerjahn, A., Kirchhoff, F., Helmchen, F., 2005. Resting microglial cells are highly dynamic surveillants of brain parenchyma in vivo. In Science. Vol. 308, ed.^eds., United States, pp. 1314-8.

Oberlander, J.G., Woolley, C.S., 2016. 17beta-Estradiol Acutely Potentiates Glutamatergic Synaptic Transmission in the Hippocampus through Distinct Mechanisms in Males and Females. J Neurosci. 36**,** 2677-90.

Orlowski, D., Soltys, Z., Janeczko, K., 2003. Morphological development of microglia in the postnatal rat brain. A quantitative study. Int J Dev Neurosci. 21**,** 445-50.

Orr, A.G., Orr, A.L., Li, X.J., Gross, R.E., Traynelis, S.F., 2009. Adenosine A(2A) receptor mediates microglial process retraction. In Nat Neurosci. Vol. 12, ed.^eds., United States, pp. 872-8.

Ramien, C., Taenzer, A., Lupu, A., Heckmann, N., Engler, J.B., Patas, K., Friese, M.A., Gold, S.M., 2016. Sex effects on inflammatory and neurodegenerative processes in multiple sclerosis. Neurosci Biobehav Rev. 67**,** 137-46.

Saijo, K., Glass, C.K., 2011. Microglial cell origin and phenotypes in health and disease. Nat Rev Immunol. 11**,** 775-87.

Saito, K., He, Y., Yan, X., Yang, Y., Wang, C., Xu, P., Hinton, A.O., Jr., Shu, G., Yu, L., Tong, Q., Xu, Y., 2016. Visualizing estrogen receptor-alpha-expressing neurons using a new ERalpha-ZsGreen reporter mouse line. Metabolism. 65**,** 522-32.

Sanchez, A.M., Flamini, M.I., Genazzani, A.R., Simoncini, T., 2013. Effects of progesterone and medroxyprogesterone on actin remodeling and neuronal spine formation. Mol Endocrinol. 27**,** 693-702.

Schafer, D.P., Lehrman, E.K., Stevens, B., 2013. The "quad-partite" synapse: microglia-synapse interactions in the developing and mature CNS. Glia. 61**,** 24-36.

Sellers, K., Raval, P., Srivastava, D.P., 2015. Molecular signature of rapid estrogen regulation of synaptic connectivity and cognition. Front Neuroendocrinol. 36**,** 72-89.

Siskova, Z., Tremblay, M.E., 2013. Microglia and synapse: interactions in health and neurodegeneration. Neural Plast. 2013**,** 425845.

Sokolowski, J.D., Mandell, J.W., 2011. Phagocytic clearance in neurodegeneration. Am J Pathol. 178**,** 1416-28.

Soltys, Z., Ziaja, M., Pawlinski, R., Setkowicz, Z., Janeczko, K., 2001. Morphology of reactive microglia in the injured cerebral cortex. Fractal analysis and complementary quantitative methods. J Neurosci Res. 63**,** 90-7.

Soltys, Z., Orzylowska-Sliwinska, O., Zaremba, M., Orlowski, D., Piechota, M., Fiedorowicz, A., Janeczko, K., Oderfeld-Nowak, B., 2005. Quantitative morphological study of microglial cells in the ischemic rat brain using principal component analysis. J Neurosci Methods. 146**,** 50-60.

Stevens, B., Allen, N.J., Vazquez, L.E., Howell, G.R., Christopherson, K.S., Nouri, N., Micheva, K.D., Mehalow, A.K., Huberman, A.D., Stafford, B., Sher, A., Litke, A.M., Lambris, J.D., Smith, S.J., John, S.W., Barres, B.A., 2007. The classical complement cascade mediates CNS synapse elimination. Cell. 131**,** 1164-78.

Tremblay, M.E., Stevens, B., Sierra, A., Wake, H., Bessis, A., Nimmerjahn, A., 2011. The Role of Microglia in the Healthy Brain. In J Neurosci. Vol. 31, ed.^eds., pp. 16064-16069.

Van Kempen, T.A., Gorecka, J., Gonzalez, A.D., Soeda, F., Milner, T.A., Waters, E.M., 2014. Characterization of neural estrogen signaling and neurotrophic changes in the Accelerated Ovarian Failure mouse model of menopause. Endocrinology. en20141190.

Villa, A., Vegeto, E., Poletti, A., Maggi, A., 2016. Estrogens, Neuroinflammation, and Neurodegeneration. Endocr Rev. 37**,** 372-402.

Wake, H., Moorhouse, A.J., Jinno, S., Kohsaka, S., Nabekura, J., 2009. Resting microglia directly monitor the functional state of synapses in vivo and determine the fate of ischemic terminals. In J Neurosci. Vol. 29, ed.^eds., pp. 3974-80.

Wright, L.E., Christian, P.J., Rivera, Z., Van Alstine, W.G., Funk, J.L., Bouxsein, M.L., Hoyer, P.B., 2008. Comparison of skeletal effects of ovariectomy versus chemically induced ovarian failure in mice. J Bone Miner Res. 23**,** 1296-303.

Wright, S.D., Jong, M.T., 1986. Adhesion-promoting receptors on human macrophages recognize Escherichia coli by binding to lipopolysaccharide. J Exp Med. 164**,** 1876-88.

Wright, S.D., Weitz, J.I., Huang, A.J., Levin, S.M., Silverstein, S.C., Loike, J.D., 1988. Complement receptor type three (CD11b/CD18) of human polymorphonuclear leukocytes recognizes fibrinogen. Proc Natl Acad Sci U S A. 85**,** 7734-8.

Young, K., Morrison, H., 2018. Quantifying Microglia Morphology from Photomicrographs of Immunohistochemistry Prepared Tissue Using ImageJ. J Vis Exp. in press.

Ziebell, J.M., Taylor, S.E., Cao, T., Harrison, J.L., Lifshitz, J., 2012. Rod microglia: elongation, alignment, and coupling to form trains across the somatosensory cortex after experimental diffuse brain injury. J Neuroinflammation. 9**,** 247.

Figure 1.

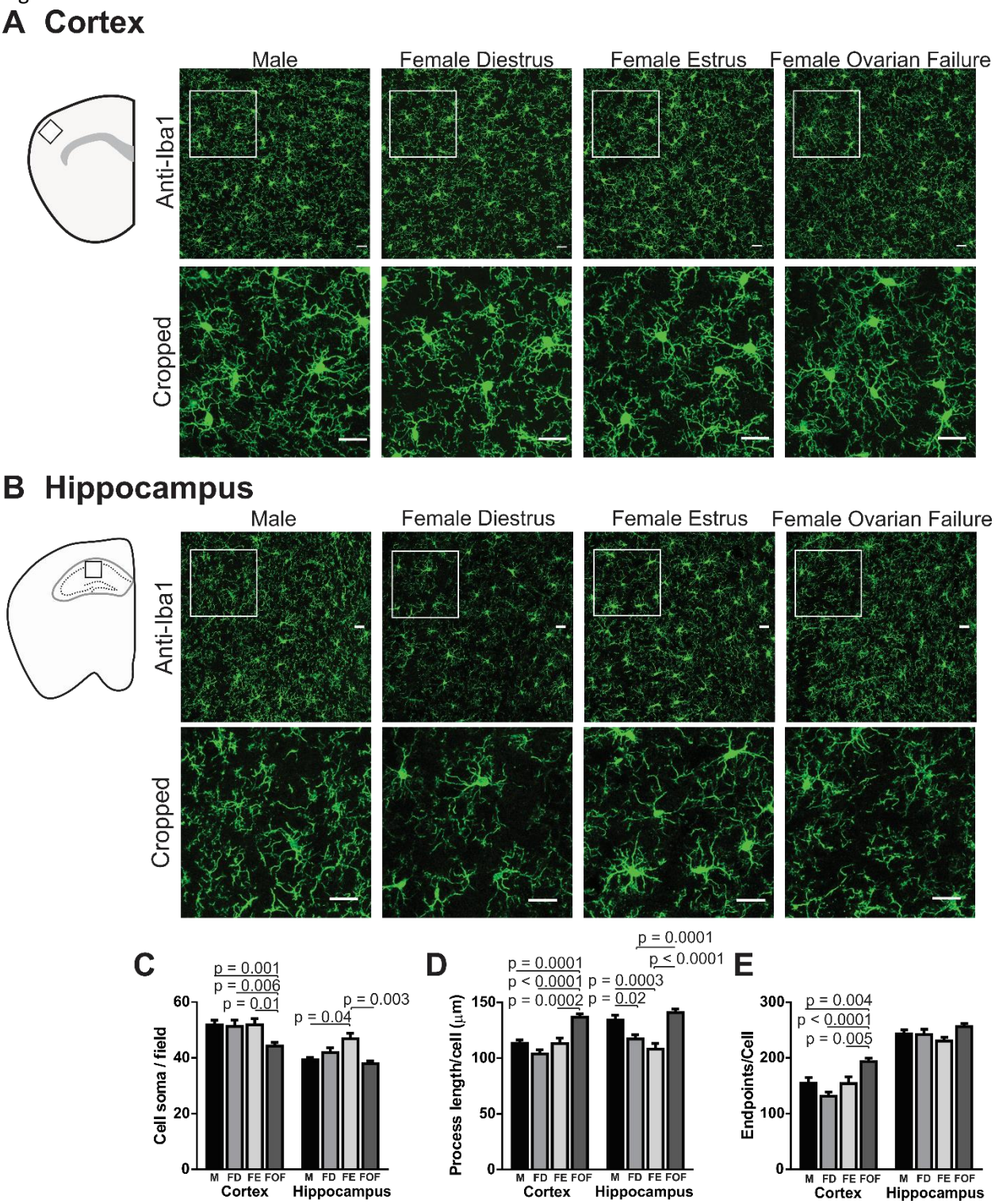
A Cortex
Male
Female Diestrus
Female Estrus
Female Ovarian Failure
Anti-Iba1
Cropped
B Hippocampus
Male
Female Diestrus
Female Estrus
Female Ovarian Failure
Anti-Iba1
Cropped
C
p = 0.001
p = 0.006
p = 0.01
p = 0.04
p = 0.003
Cell soma / field
60
40
20
0
M FD FE FOF
Cortex
M FD FE FOF
Hippocampus
D
p = 0.0001
p < 0.0001
p = 0.0002
p = 0.0003
p = 0.02
p = 0.0001
p < 0.0001
Process length/cell (µm)
150
100
50
0
M FD FE FOF
Cortex
M FD FE FOF
Hippocampus
E
p = 0.004
p < 0.0001
p = 0.005
Endpoints/Cell
300
200
100
0
M FD FE FOF
Cortex
M FD FE FOF
Hippocampus

Figure 2.

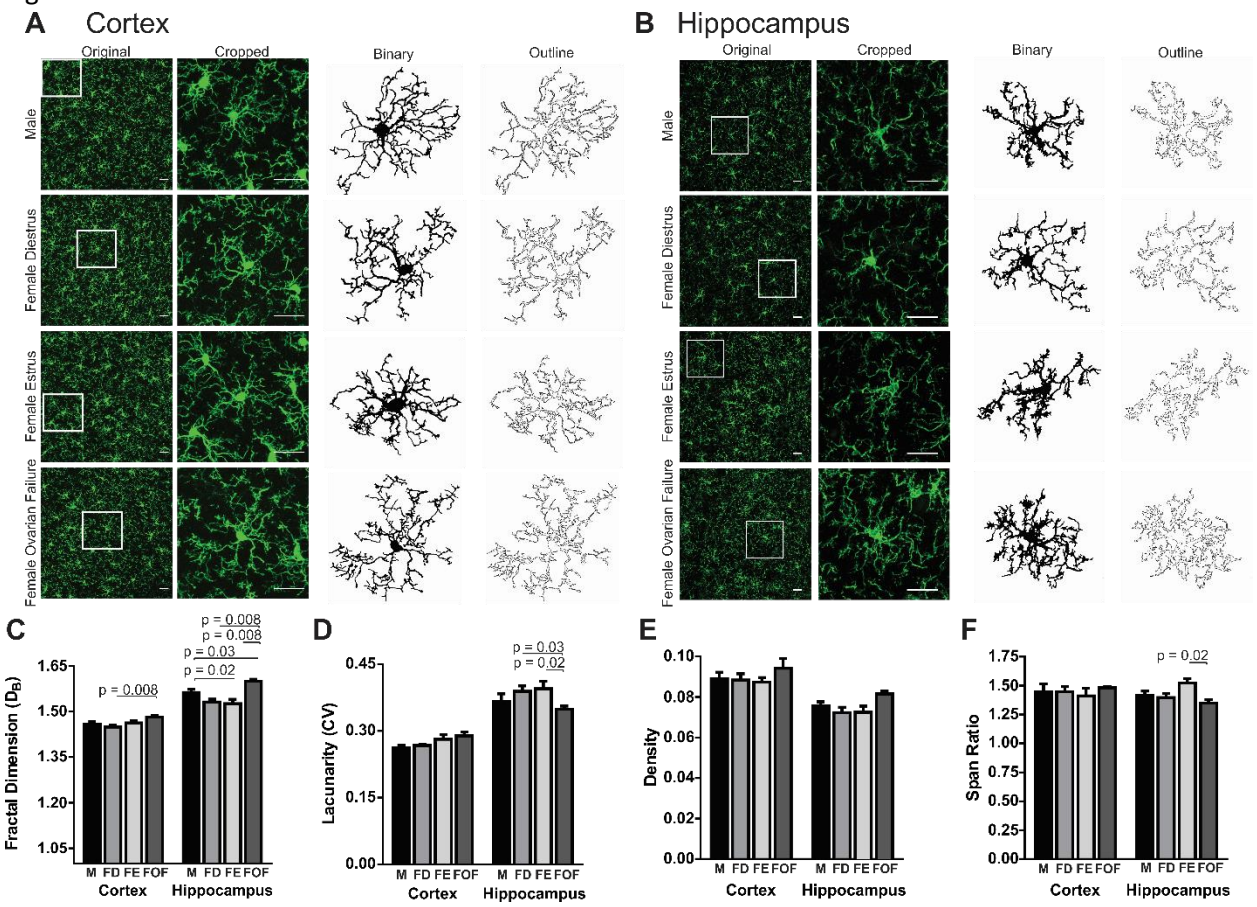
A Cortex
B Hippocampus
Original
Cropped
Binary
Outline
Male
Female Diestrus
Female Estrus
Female Ovarian Failure
C
Fractal Dimension (D_B)
p = 0.008
p = 0.008
p = 0.03
p = 0.02
D
Lacunarity (CV)
p = 0.03
p = 0.02
E
Density
F
Span Ratio
p = 0.02
M FD FE FOF
Cortex
Hippocampus

Figure 3.

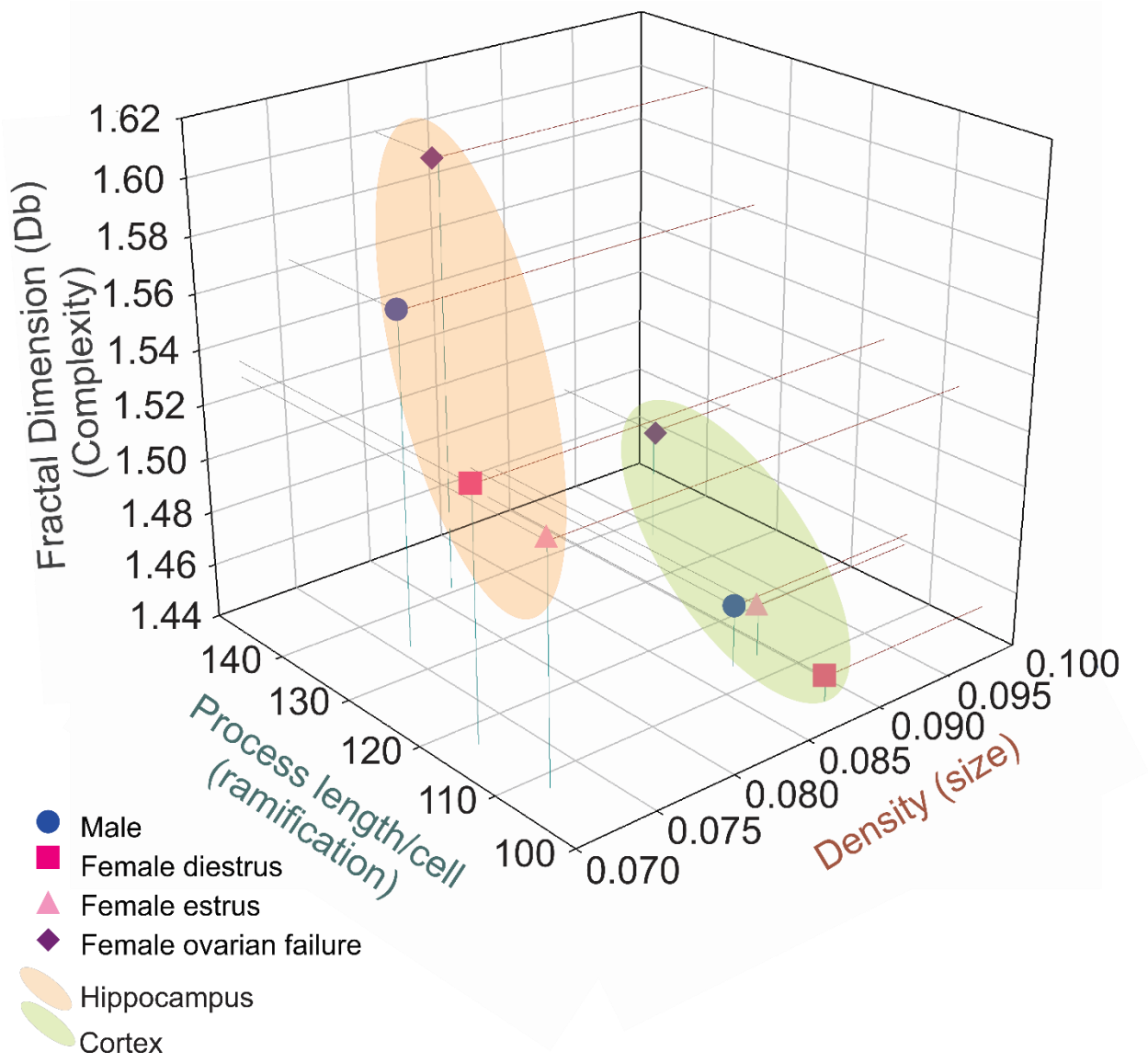

Figure 4.

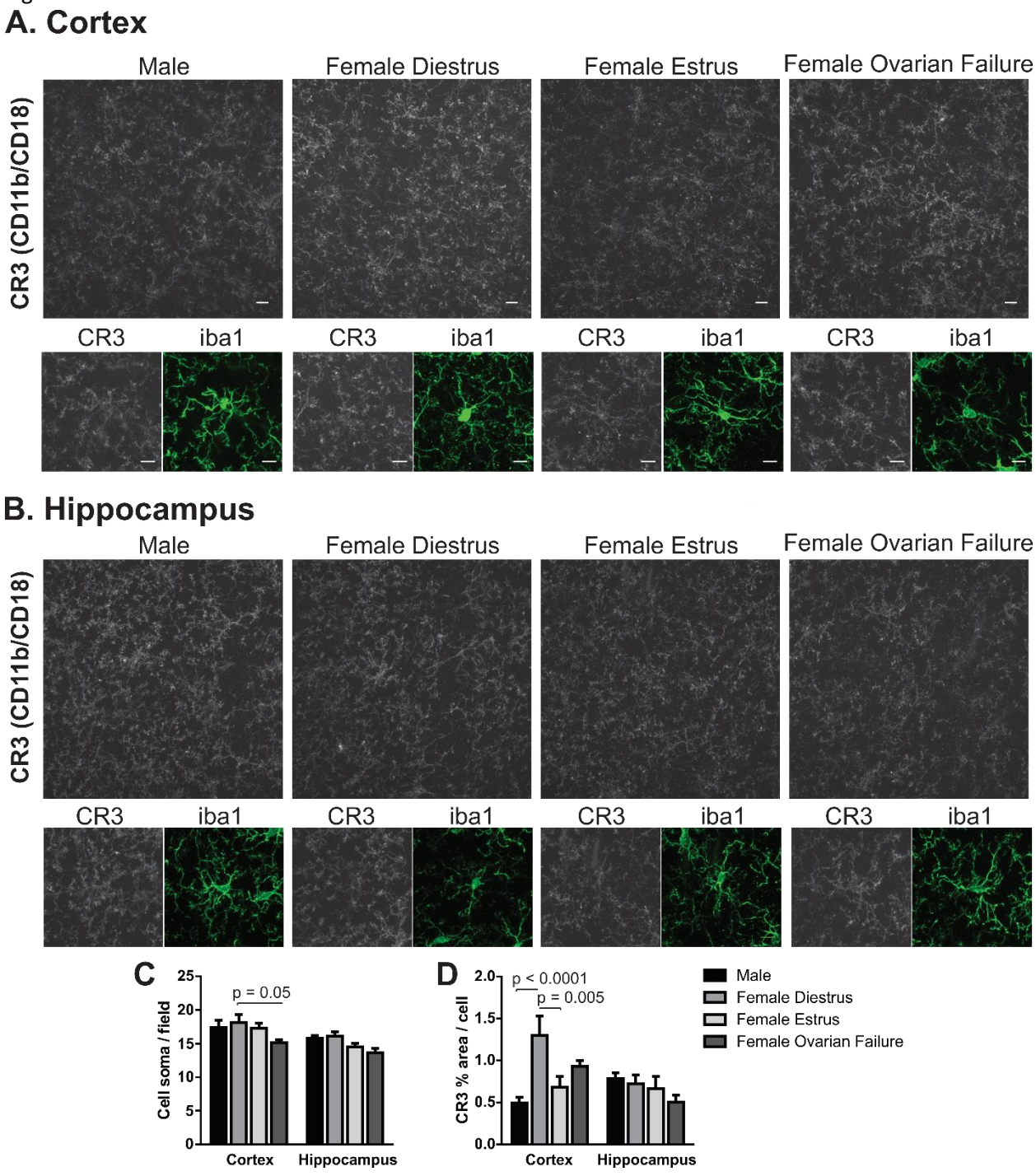
A. Cortex
Male
Female Diestrus
Female Estrus
Female Ovarian Failure
CR3 (CD11b/CD18)
CR3
iba1
B. Hippocampus
C
Cell soma / field
p = 0.05
Cortex
Hippocampus
D
CR3 % area / cell
p < 0.0001
p = 0.005
Male
Female Diestrus
Female Estrus
Female Ovarian Failure

Figure 5

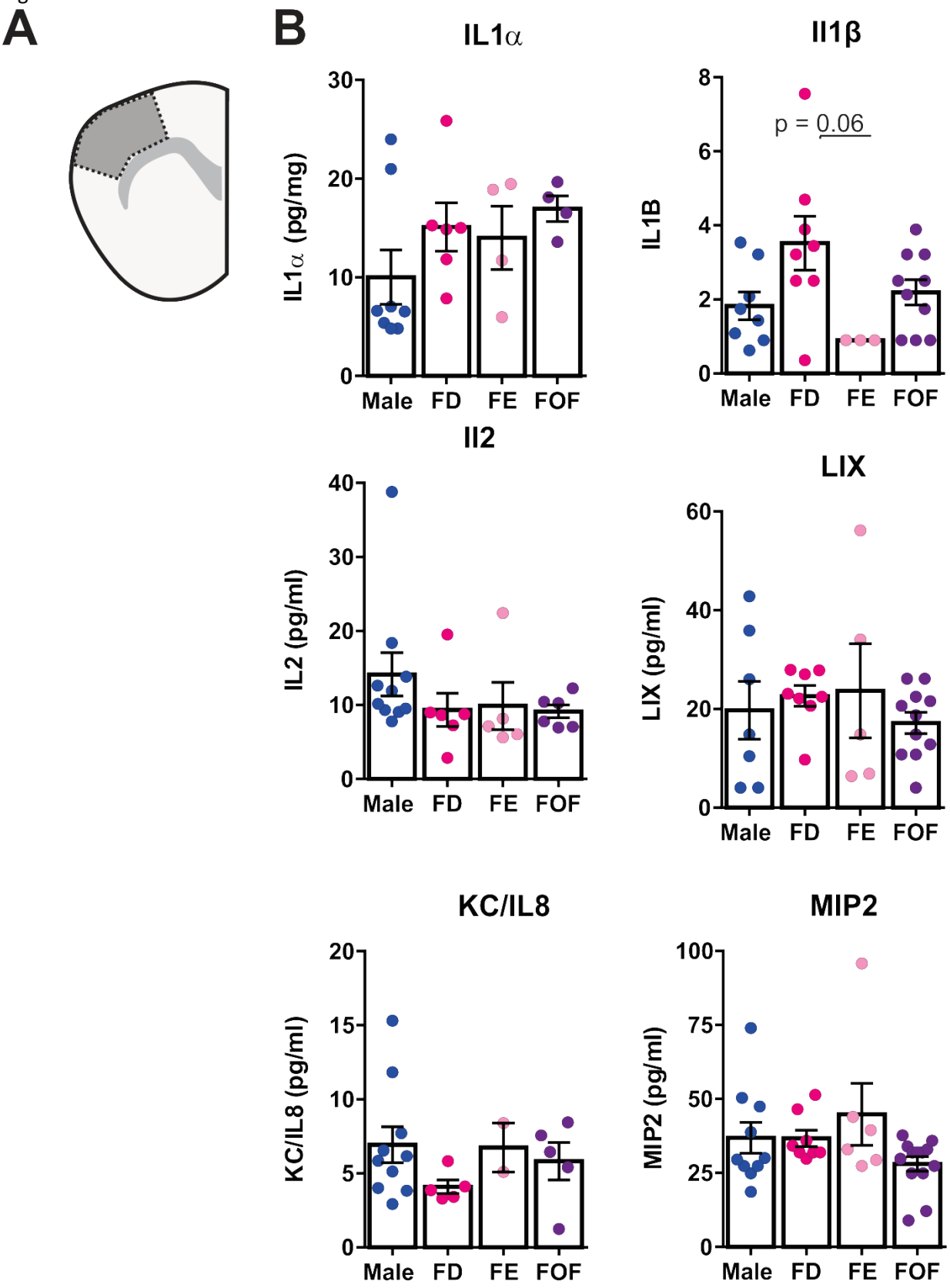

Additional Figure 1.

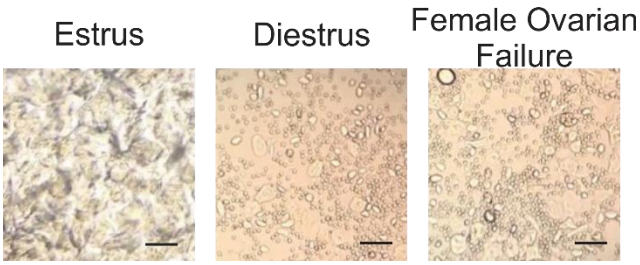

Additional Figure 2.

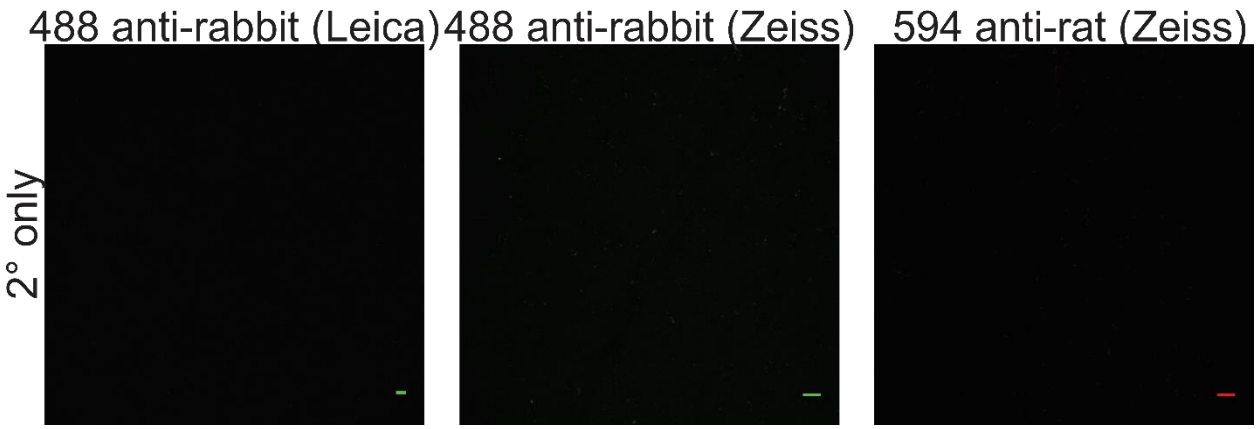

Additional Figure 3.

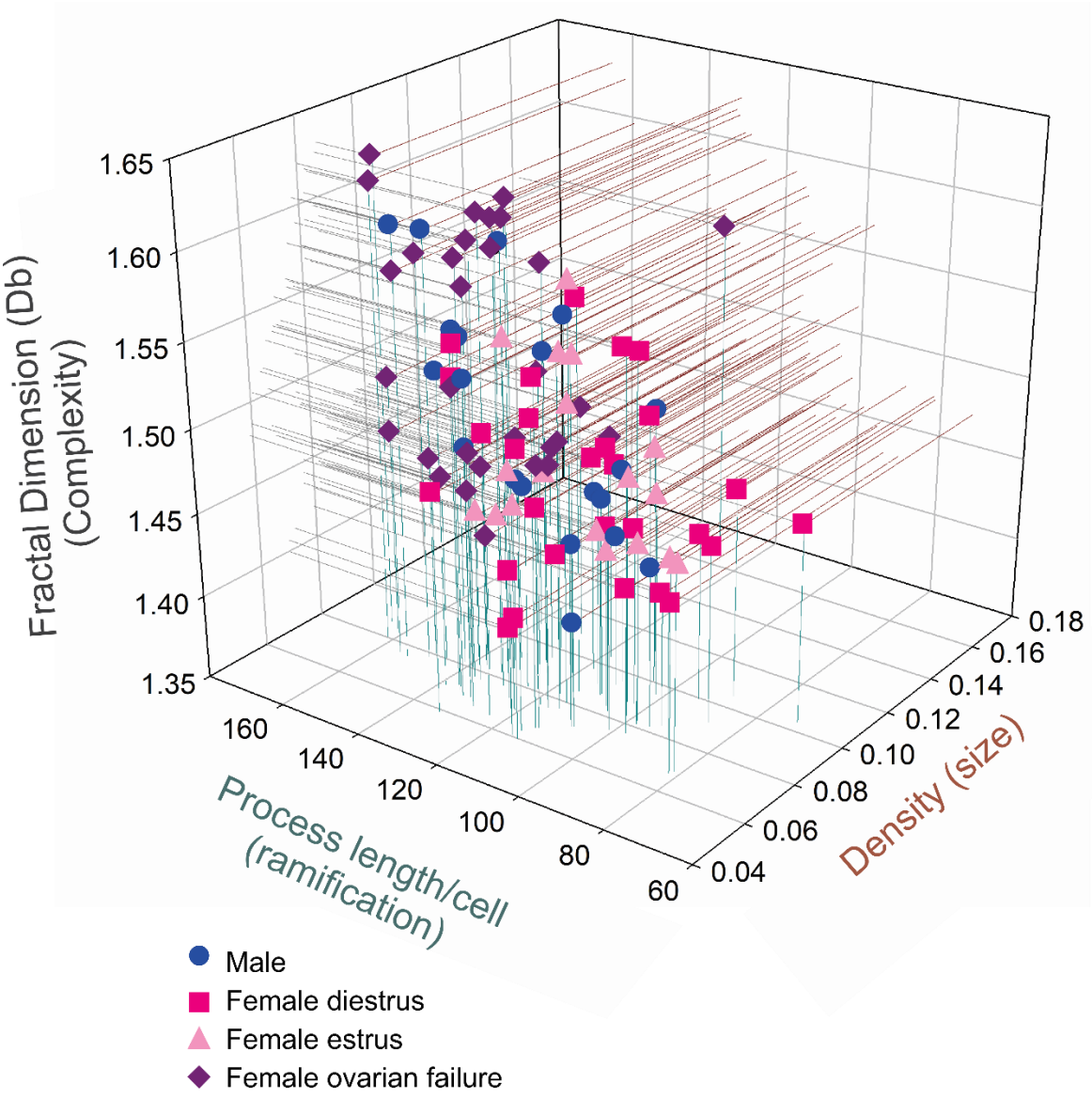

Additional Table 1.

	Standard Curve Range (pg/ml)		PLATE CONTROLS				EXPERIMENT POSITIVE CONTROL		
Analyte	Low	High	expected value low range (pg/ml)	Measured (pg/ml)	expected value high range (pg/ml)	Measured (pg/ml)	Injured brain measured (pg/ml)	SEM	n (27)
GM-CSF	6.35	1499.5	171-355	293.8	688-1429	1185.3	9.1	1.2	5
INFy	0.49	2036.8	15-31	20.9	60-125	89.5	0.5	0.1	10
IL1a	3.90	68384.9	82-169	108.1	340-706	508.2	24.9	3.5	21
IL1B	3.92	4118.5	97-201	138.3	407-846	635.7	3.1	0.4	24
IL2	0.98	3864.6	18-37	12.5	70-145	51.2	10.1	0.7	21
IL4	0.10	402.9	2.8-5.7	4.5	10--22	20.3	0.1	0.0	23
IL5	0.97	4260.1	32-67	49.9	133-276	236.6	2.9	8.3	17
IL6	1.01	3942.5	33-68	49.4	133-276	208.5	1666.0	390.4	23
IL7	2.03	1980.6	14-29	15.0	51-105	59.0	0.2	1.0	10
IL10	1.34	5521.5	49-101	64.5	192-398	283.0	1.4	0.4	6
IL12	2.93	3024.8	62-130	71.0	242-502	283.6	1.7	0.3	6
IL13	3.47	15518.4	124-258	177.0	471-977	812.8	1.7	8.0	16
LIX	3.20	13166.9	86-179	56.4	316-656	249.4	88.2	17.5	24
IL17A	0.49	2065.0	16-34	23.2	68-171	97.0	0.5	0.1	18
KC	0.75	3019.5	36-76	51.9	147-306	237.5	462.8	111.9	23
MCP1	3.95	25314.7	87-181	116.1	365-758	506.1	347.1	74.1	25
MIP2	7.32	1875.2	382-793	258.4	1451-3014	1248.7	361.8	83.5	27
TNFα	0.50	510.3	13-27	19.7	53-110	92.0	2.8	0.7	19

PeerJ Preprints | https://doi.org/10.7287/peerj.preprints.26937v1 | CC BY 4.0 Open Access | rec: 16 May 2018, publ: 16 May 2018